ACS APPLIED MATERIALS & INTERFACES

Research Article

www.acsami.org

Nanoconfinement Induced Formation of Core/Shell Structured Mesoporous Carbon Spheres Coated with Solid Carbon Shell

Karolina Wenelska,[†] Krzysztof Kierzek,[‡] Ryszard J. Kaleńczuk,[†] Xuecheng Chen,*[,†] and Ewa Mijowska*[,†]

[†]Institute of Chemical and Environment Engineering, West Pomeranian University of Technology, Szczecin, ul. Pulaskiego 10, 70-322 Szczecin, Poland

[‡]Department of Polymer and Carbonaceous Materials, Wroclaw University of Technology, ul. Gdanska 7/9, 50-344 Wroclaw, Poland

Supporting Information

ABSTRACT: A novel method for the fabrication of core/shell structured mesoporous carbon spheres with solid shell using a template method has been presented. The unique molecular nanostructures are characterized by XRD, TEM, TGA, and nitrogen adsorption/desorption measurement. The formation mechanism of the mesostructured carbon spheres with a carbon shell is proposed according to the experimental results. Nanoconfinement effect, occurring in the core/shell structured template, is believed to play a key role in mediating the formation of these hierarchical carbon mesostructures, with SnO_2 as a template and C_2H_4 as a carbon source of a mesoporous carbon core. This synthesis method is simple, straightforward, and suitable for the preparation of various nanostructures that are unique scaffolds in catalytic and electrochemical applications.

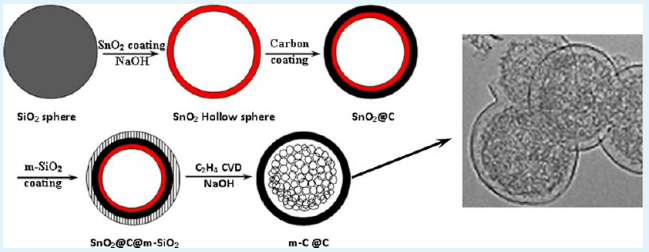

KEYWORDS: *mesoporous, hollow, tin oxide, hydrothermal, core/shell, lithium ion battery*

1. INTRODUCTION

Graphitic nanostructured carbons, such as carbon spheres, have been the subject of considerable attention from both scientific and practical application aspects. In particular, carbon spheres with hollow cores and porous shells combine properties of hollow carbon spheres and porous structures and they are particularly fascinating due to their low density, high surface area, large pore volume, chemical inertness, good mechanical stability and surface permeability. These properties make them suitable for several potential applications including adsorbents, sensors, storage materials, catalyst supports, supercapacitors, and fuel cell electrodes.[1−9]

Porous carbon materials, another kind of porous structured materials,[10−12] also have recently attracted much attention due to their many advanced applications, which include their use as catalysts, separation systems, low-dielectric constant materials, photonic crystals, templates for the synthesis of inorganic nanostructures, and hydrogen storage materials.[13−19] There are numerous ways to synthesize porous carbons including (1) physical activation of carbon to high burnoff degree,[20] (2) combination of physical and chemical activation,[21] (3) carbonization of polymer blends with one unstable component,[22] (4) carbonization of polymer aerogels[23] or cryogels,[24] (5) templating with mesoporous silica,[25] and (6) direct carbonization of metal−organic frameworks in innert atmosphere.[26] The templating with mesoporous silica is particularly attractive, and it is a method widely used to prepare mesoporous carbons now since 2002 when Yoon has first reported synthesis of monodispersed mesoporous hollow carbon spheres from solid core mesoporous silica spheres and hollow mesoporous aluminosilicate spheres templates.[27,28] Although there are many reports on the preparation of different kinds of hollow carbon spheres. To the best of our knowledge, a route for synthesis of core/shell structured carbon spheres with mesoporous core and solid shell has not been reported so far.

Lithium ion batteries (LIBs), which power most of today's portable electronic devices, have been actively investigated as energy sources for transportation applications. To date, graphite has been the most commonly used anode material in commercial LIBs because of its low cost, low lithium intercalation potential, and good cyclic stability.[29] However, graphite's limited Li intercalation capacity (LiC_6, 372 mAh/g) and poor rate performance induced by its low Li diffusion coefficient have hindered its application in electric vehicles (EVs) and hybrid electric vehicles (HEVs). However, bulk carbonaceous materials suffer from slow lithium diffusion rates within their frameworks, thus limiting their rate capabilities.[30] Improvements have been made by introducing mesopores to these frameworks,[31] which not only reduce the solid-state diffusion pathway for Li^+ but also provide fast transport channels for conducting ions. Consequently, porous electrode materials have higher capacities and much faster rate performances than their corresponding bulk counterparts.[32] Mesoporous based carbons[33,34] have also been tested as anode materials for LIB.[35−37] These carbon materials exhibited high

Received: December 15, 2012
Accepted: March 15, 2013
Published: April 5, 2013

lithium storage capacity and good rate capabilities. However, the electronic conductivity of the final carbons is relatively low. Recently, the "brick and mortar" approach to the synthesis of soft-template carbons with improved electronic conductivity was reported for the coassembly of phenolic resins with graphitic nanostructures, namely, onionlike carbons and carbon black.[38]

Following a similar rationale, herein we report the template synthesis method for mesoporous carbon spheres coated with solid graphitic shells. The present results show the improved electronic and surface properties of the final nanocomposites as anode materials for lithium ion batteries, mitigating the key issue related to the low electronic conductivity of hard mesoporous carbons synthesized via low-temperature carbonization.

2. EXPERIMENTAL SECTION

2.1. Synthesis of SiO_2 Spheres. SiO_2 nanospheres were prepared by a modified Stöber sol–gel process.[39] Tetraethyl orthosilicate (TEOS) (1.5 mL) was added to a mixture of ethanol (50 mL) and concentrated ammonia (28 wt %, 2.5 mL). Then the solution was stirred for another 24 h. Afterward, 0.5 g of the products was separated by filtration, washed with ethanol, and dried in vacuum.

2.2. Preparation of SnO_2 Hollow Spheres. In a typical synthesis, 80 mg of prepared SiO_2 spheres were dispersed in 1.3 mL of water by ultrasonication; 0.6 g of urea and 0.09g of $Na_2SnO_3{\cdot}3H_2O$ were dissolved in 11.3 mL of DI water. Then 6 mL of ethanol was added to the solution to form milky suspension under mild stirring. These two suspensions were mixed and transferred to a 25 mL Teflon autoclave and heated in an electric oven at 170 °C for 36 h. After the autoclave was cooled down to room temperature, the product was filtrated and washed with DI water. About 130 mg of dry SiO_2@SnO_2 product was obtained. The SiO_2 core was etched in 2 M of NaOH, and the remaining material was filtrated again and dried in an oven at 100 °C, and finally, 62 mg of hollow SnO_2 was collected.

2.3. Synthesis of SnO_2 @Carbon Hollow Spheres. A total of 62 mg of SnO_2 hollow spheres was coated with carbon through hydrothermal reaction. In a typical synthesis, SnO_2 hollow spheres were dispersed in 16 mL of H_2O, 4 mL of ethanol, and 0.4 g of glucose. Then the mixture was transferred to the autoclave. The reaction temperature was 190 °C, and time was set to 36 h. After this reaction, 100 mg of SnO_2@C was obtained.

2.4. Preparation of SnO_2@Carbon@m-SiO_2. The 100 mg of SnO_2@Carbon spheres, obtained in the previous step, was first dispersed in the solution containing 50 mL of H_2O, 40 mL of ethanol, 0.15 g of cetyl trimethylammonium bromide (CTAB), and 0.6 mL of $NH_3{\cdot}H_2O$ with ultrasonication. After 30 min, 0.150 mL of TEOS was added and the mixture was vigorously stirred for 24 h. The mixture was filtrated and washed with distilled water and ethanol. Afterward, the obtained product (280 mg) was dried at 60 °C for 8 h.

2.5. m-C@Carbon Spheres Synthesis. SnO_2@Carbon@m-SiO_2 spheres (280 mg) were placed in an alumina boat and set in a tube furnace. CVD was applied, and Ar and C_2H_4 were introduced in a flow rate of 100 and 30 sccm, respectively. The synthesis temperature was set to 800 °C, and the reaction time was 3 h. At last, 50 mg of m-C@Carbon spheres was obtained.

2.6. Characterization. Transmission electron microscopy (TEM) was conducted together with energy dispersive X-ray spectrometer as its mode has been utilized to examine the dimensions, structural details, and chemical composition of the samples (Tecnai F30 with a field emission gun operating at 200 kV). X-ray diffraction (XRD) was conducted on a Philips diffractometer using Cu Kα radiation. Thermogravimetric analysis (TGA) was carried out on 10 mg samples using the DTA-Q600 SDT TA Instrument at a heating rate of 10 °C/min from room temperature to 900 °C under air. The specific surface area was calculated by the Brunauer–Emmett–Teller (BET) method via a Micromeritics ASAP 2010 M instrument. The pore size distribution was determined using the Barrett–Joyner–Halenda (BJH) method.

2.7. Electrochemical Measurements. The electrochemical experiments were carried out using 2032 coin-type cells. The working electrodes were prepared by mixing the hollow carbon spheres, carbon black (C-NERGY SUPER C65, Timcal), and polyvinylidene difluoride (PVDF, Solef 5130, Solvay) at a weight ratio of 80:10:10 and pasting onto Cu foils (Schlenk Metallfolien GmbH & Co.). A lithium foil (Aldrich) was used as the counter electrode. The electrolyte consisted of a solution of 1 M $LiPF_6$ in ethylene carbonate (EC)/dimethyl carbonate (DMC) (1:1 by volume) obtained from Merck Chemicals (SelectiLyte LP30). The cells were assembled in an argon-filled glovebox with less than 1 ppm moisture and oxygen. The electrochemical performance was evaluated in the voltage range of 0.005–2.0 V by using a galvanostatic charge/discharge technique at a rate of C/5.

3. RESULTS AND DISCUSSION

A scheme of synthesis route of m-@C spheres is shown in Figure 1. First, solid silica spheres were coated with SnO_2 through hydrothermal reaction and then removed SiO_2 by NaOH solution. After this procedure, SnO_2 hollow spheres were obtained. Thereafter, a carbon layer with a thickness of 35 nm was deposited on the surface of the SnO_2 hollow sphere by the hydrothermal reaction. The SnO_2 hollow spheres coated with carbon were then coated with another mesoporous silica layer through sol–gel process. In the last step, SnO_2 spheres coated with carbon and mesoporous silica were put into tube furnace and mesoporous carbon spheres with solid shell were finally obtained through CVD reaction. SnO_2 and SiO_2 components were also removed by refluxing in concentrated NaOH solution.

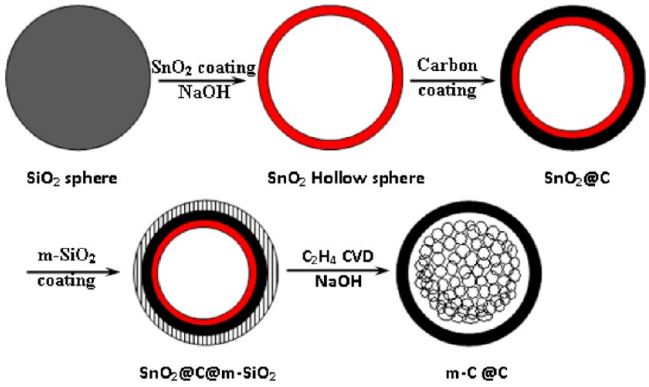

Figure 1. Scheme of the procedure for the synthesis of porous carbon spheres with solid carbon shell.

The experimental procedures and the observations are summarized in Figure 2 and Supporting Information Figure S1. TEM images show that solid SiO_2 nanospheres obtained by a modified Stöber sol–gel process are monodispersed and the mean diameter is ca. 200 nm (Figure 2a). The SiO_2@SnO_2 spheres from hydrothermal reactions are shown in images (Figure 2c, d and Figure S1a). The SnO_2 hollow spheres were prepared by removal of the silica component as described previously.[40,41] The SnO_2 nanoparticles have a mean diameter of about 300 nm and consist of nanoparticles with the diameter of 15 nm on the sphere surface. After coating with a nonporous carbon layer, hollow structured SnO_2@C spheres with a thin carbon layer of ca. 20 nm were obtained (Figure 2e, f and Figure S1b). As shown in SEM images from Figure S1b, SnO_2@C spheres are hollow structures. Further deposition of

dx.doi.org/10.1021/am303124t | ACS Appl. Mater. Interfaces 2013, 5, 3042–3047

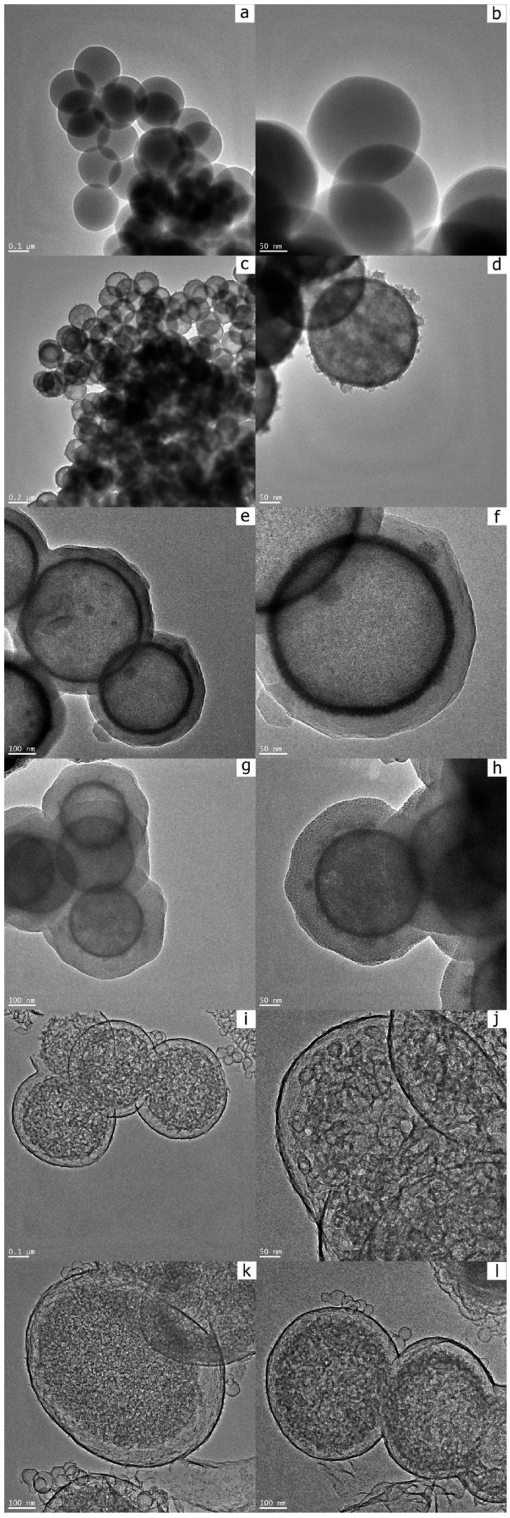

Figure 2. TEM images of (a, b) solid SiO_2 spheres, (c, d) SiO_2@SnO_2 spheres, (e, f) SnO_2@C spheres, (g, h) SnO_2@C@m-SiO_2 spheres, and (i–l) m-C@Carbon spheres.

mesoporous silica resulted in a sample, SnO_2@C@m-SiO_2, presented in Figure 2g, h and Figure S1c. A typical sandwich structure with a hollow core, a nonporous carbon layer in the middle layer, and an ordered mesoporous silica phase with cylindrical channels in the outer layer can be clearly observed. Interestingly, the mesopore channels are found to be perpendicular to the sphere surface (Figure 2g, h and Figure 1Sc). Images depicted in TEM images from Figure 2i–l and SEM images from Figure S1e, f present the final product of m-C@Carbon sphere; some spheres are broken, which means that these spheres are hollow structures. Combining the results from TEM in Figure 2i–l, it can be concluded that these spheres are core/shell structures. Here, one can see that the spherical structure of the samples changed the diameter up to 400 to ~510 nm. These spherical particles are core/shell structured spheres as revealed by the contrast between the dark edge and pale center in the spheres as well (Figure 2j, k). The shells of these carbon spheres have a thickness of about 10 nm. The higher magnification TEM image in Figure 2j reveals porous structures composed of the similar small hollow carbon sphere in the core, and the pore size is about 3 nm.

To investigate the porosity structural properties of m-C@Carbon spheres N_2, adsorption/desorption measurements were used. The N_2 adsorption/desoption isotherms at 77 K for m-C@Carbon spheres and their corresponding pore size distributions are shown in Figure 3; the curve indicates that the pore sizes are in the mesoporous range. The specific surface area and total pore volume of mesoporous m-C@Carbon spheres are 543 m^2/g and 0.0446 cm^3/g, respectively (Figure 3a). The corresponding pore size distribution calculated using the BJH method from the adsorption branch reveals the pores centered at 1.22, 1.48, 2.65, and 3.78 nm. From the above N_2 sorption/desorption results, it can be concluded that our core/shell structured carbon spheres are mesoporous in structure. The specific surface area and total pore volumes of other samples are also listed in Table S1 in the Supporting Information.

The XRD patterns of m-C@Carbon spheres are shown in Figure 4A. The strong peaks at 25° and 43° are assigned to a graphitic carbon, which indicate that the mesoporous structures are composed of graphitic carbon; there is also a little amount of SnO_2 remaining in the mesoporous carbon spheres, which comes from the SnO_2 template. Carbon can also be detected from other samples, for example, SnO_2@C@m-SiO_2/C, SnO_2@C@ m-SiO_2, and SnO_2@C spheres. Prior to annealling in Ar, four types of materials exhibit broad peaks due to very small particulate SnO_2. After the CVD process, the strong diffraction peaks are observed from the samples of SnO_2@C@ m-C and SnO_2@C@m-SiO_2@C, indicating the increase in crystallinity of the SnO_2 phase. Ideal graphite starts to oxidize at above 600 °C. As shown in Figure 4B, the m-C@Carbon spheres presented here began to decompose at 561 °C in air. As the temperature is further increased, the weight loss increases rapidly until all of the m-C@Carbon spheres are exhausted at about 584 °C. The ash content (15 wt %) comes from SnO_2 or trace amounts of silica template. TGA profiles for SnO_2@C, SnO_2@C@m-SiO_2, SnO_2@C@m-SiO_2@C, and SnO_2@C@m-C are also shown in Figure 4. The ash contents are 80, 58, 75, and 65 wt % for SnO_2@C, SnO_2@C@m-SiO_2, SnO_2@C@m-SiO_2@C, and SnO_2@C@m-C, respectively.

To investigate the mechanism for the formation of core/shell mesoporous structured carbon spheres, another two parallel experiments have been conducted. Hollow SnO_2 spheres and SnO_2@C hollow spheres were treated under the same CVD conditions as SnO_2@C@m-SiO_2 spheres. TEM analysis was used to investigate the morphological differences among three samples after CVD reactions. Figure 5a shows the SnO_2 hollow structure before CVD process. In Figure 5b, one can see SnO_2 spheres after CVD reaction. After this process, hollow sphere structures have been completely destroyed; only small tin

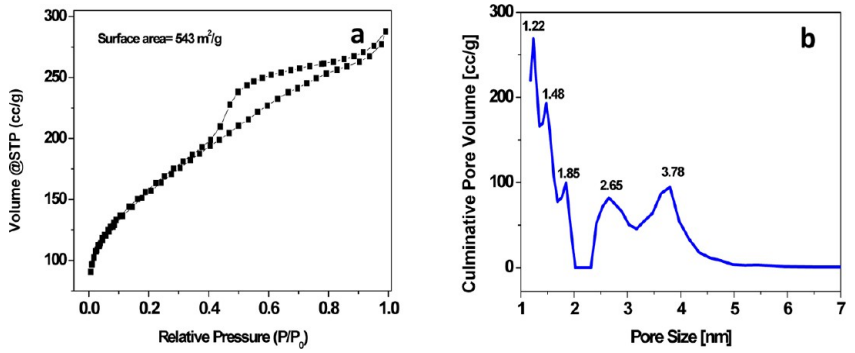

Figure 3. (a) Nitrogen adsorption/desportion isotherm of m-C@Carbon spheres. (b) Pore size distributions of m-C@Carbon spheres.

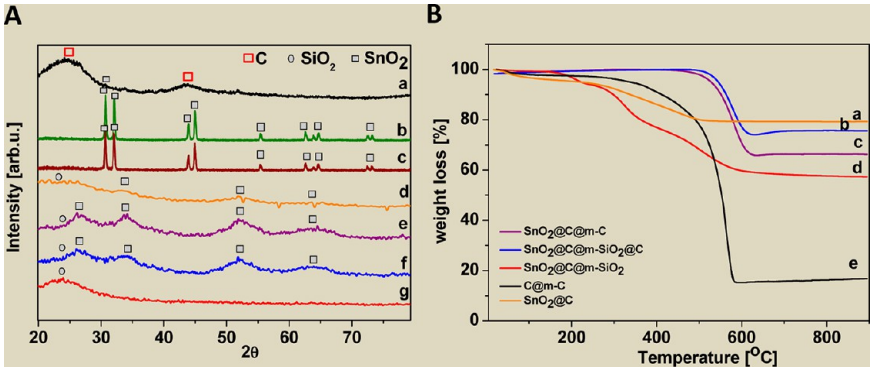

Figure 4. (A) XRD patterns of core/shell structured spheres: (a) m-C@Carbon spheres, (b) SnO_2@C@m-Cspheres, (c) SnO_2@C@m-SiO_2@C spheres, (d) SnO_2@C@m-SiO_2 spheres, (e) SnO_2@C spheres, (f) SiO_2@SnO_2 spheres, and (g) solid SiO_2 spheres. (B) TGA profiles of (a) SnO_2@C spheres, (b) SnO_2@C@m-SiO_2@C spheres, (c) SnO_2@C@m-C spheres, (d) SnO_2@C@m-SiO_2 spheres, and (e) m-C@Carbon spheres.

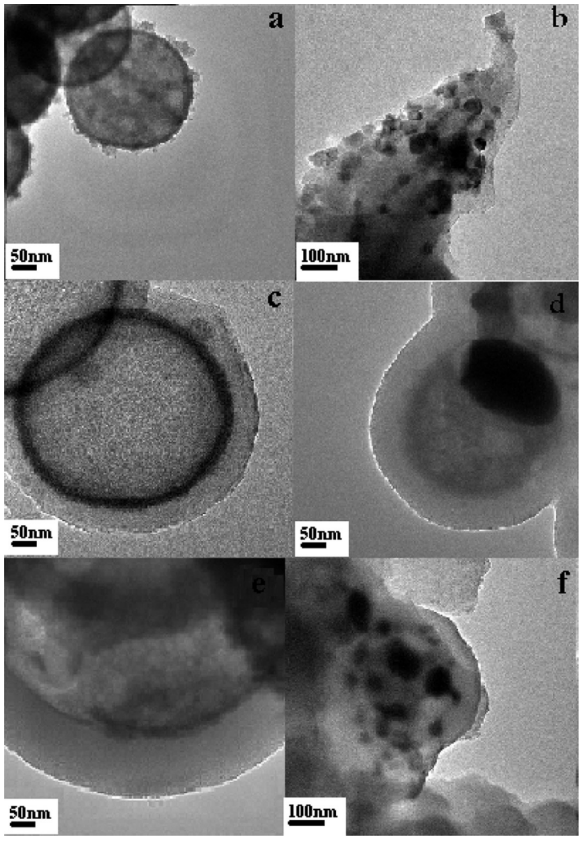

Figure 5. TEM images of hollow spheres and corresponding CVD products: SnO_2 (a, b), SnO_2@C (c, d), and hollow spheres (e, f).

particles in carbon matrix can be seen, and the Sn particles have been coated by carbon. Figure 5c and d presents TEM images of SnO_2@C spheres before and after CVD. After the CVD process, SnO_2 was also reduced to Sn, forming big particles trapped in carbon spheres. Only the SnO_2@C@m-SiO_2 spheres kept their own structure after the CVD process (Figure 5f). Inside these spheres, there are many small tin nanoparticles coated by carbon. After removal the Sn nanoparticles, the core/shell structured hollow carbon spheres were obtained. It is very important to use the CVD process at the right moment to prevent structure destruction. Comparing the CVD results of SnO_2@C and SnO_2@C@m-SiO_2 spheres, it can be seen that the existence of mesoporous silica structure on carbon shell plays a key role in the formation of core/shell structured hollow carbon spheres. The mesoporous silica shell can harvest C_2H_4 molecules and let them slowly get inside the hollow spheres, finally forming the Sn@C small nanoparticle structure. The difference in these three samples stands for the presence of carbon and mesoprous silica shell. They are very important for the formation of mesoporous carbon core. So, from above experimental results, we proposed that the nanoconfinement effect induced the formation of mesoporous carbon core.

To test the electrochemical properties of m-C@Carbon spheres, they were used as anode materials for lithium ion battery. Galvanostatic discharging (Li insertion)−charging (Li extraction) experiments are performed on m-C@Carbon spheres. Another phenolic resin derived activated carbon (A-PhR) was tested as reference material. The A-PhR shows a BET surface area of 585 m^2/g, which is very similar to porosity development of m-C@Carbon spheres. However, a mean micropore size of 0.7 nm suggests that A-PhR is an

dx.doi.org/10.1021/am303124t | ACS Appl. Mater. Interfaces 2013, 5, 3042−3047

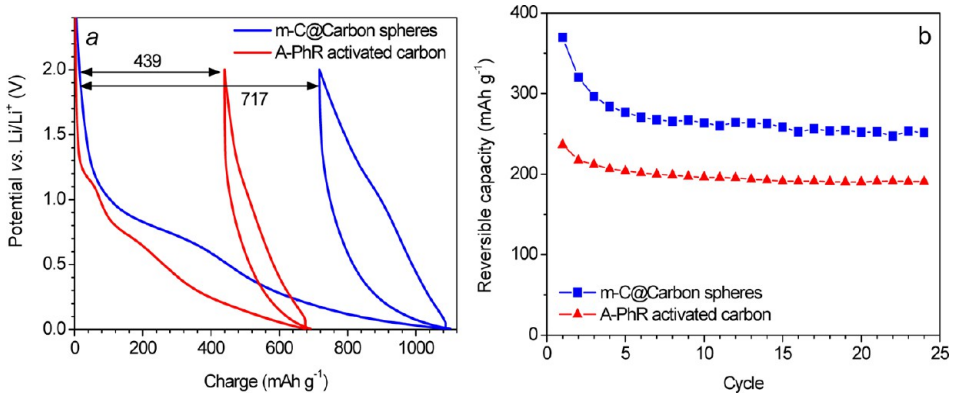

Figure 6. First charge/discharge curves (a) and electrochemical stability (b) of the m-C@Carbon spheres and reference activated carbon (A-PhR).

outstandingly microporous solid. As presented in Figure 6a, the first charge capacity as high as 370 mAh/g is observed. This is over 60% higher than the capacity of A-PhR as conventional microporous activated carbon. The better performance of m-C@Carbon spheres can be attributed to the mesoporous structures which are responsible for such high capability pertaining to reversible Li insertion. However, a large irreversible capacity of about 717 mAh/g is also observed from the m-C@Carbon spheres electrode during the first discharging and charging processes, as a effect of lithium trapping in the disordered carbon structure. The cycle life of the m-C@Carbon spheres is shown in Figure 6b. The reversible capacity is almost stable at 251 mAh/g after 20 cycles. In the same conditions, the A-PhR electrode shows noticeable lower performance. It is believed that the mesoporous cores in carbon spheres are responsible for the excellent capability for Li insertion. However, owing to the larger irreversible capacity, introducing highly gravimetric and volumetric capacity materials (SnO_2 and Co_3O_4) inside of m-C@Carbon spheres may improve the reversible capacity further and these kinds of studies are currently in progress in our laboratory.

4. CONCLUSION

We demonstrate a novel method for the fabrication of core/shell structured mesoporous carbon spheres with a solid shell using a template method. The formation mechanism of the hierarchically mesostructured carbon spheres with a carbon shell is also investigated. Synergistic SnO_2, C_2H_4 carbon source, and carbon/mesoporous shell on the sphere template are believed to play a key role in mediating the formation of these hierarchical carbon mesostructures, and the SnO_2 can act as template and C_2H_4 as the carbon source for the formation of a mesoporous carbon core. This synthesis method is simple, straightforward, and suitable for the preparation of other nanostructures that are unique scaffolds in catalytic and electrochemical applications. The final core/shell mesoporous structured carbon spheres were investigated as the anode materials for lithium battery and showed improved results with respect to conventional microporous carbon.

■ ASSOCIATED CONTENT

Supporting Information

Figure showing SEM images of mesoporous carbon spheres; table showing surface area and pore volume data for mesoporous carbon spheres. This material is available free of charge via the Internet at http://pubs.acs.org.

■ AUTHOR INFORMATION

Corresponding Author

*E-mail: xchen@zut.edu.pl (X.C.); emijowska@zut.edu.pl (E.M.).

Notes

The authors declare no competing financial interest.

■ ACKNOWLEDGMENTS

This work was supported by the National Science Centre, Poland within the project no 2011/03/D/ST5/06119.

■ REFERENCES

(1) Guo, L.; Zhang, L.; Zhang, J.; Zhou, J.; He, Q.; Zeng, S.; Cui, X.; Shi, J. *Chem. Commun.* **2009**, 6071−6073.
(2) Fang, B.; Kim, M.; Yu, J. *Appl. Catal., B* **2008**, *84*, 100−105.
(3) Chai, G.; Yoon, S.; Kim, J.; Yu, J. *Chem. Commun.* **2004**, 2766−2767.
(4) Zhang, L.; Zhao, X. *Chem. Soc. Rev.* **2009**, *38*, 2520−2531.
(5) Titirici, M.; Antonietti, M. *Chem. Soc. Rev.* **2010**, *39*, 103−116.
(6) Fang, B.; Kim, J.; Kim, M.; Yu, J. *Phys. Chem. Chem. Phys.* **2009**, *11*, 1380−1387.
(7) Valdés-Solís, T.; Valle-Vigón, P.; Sevilla, M.; Fuertes, A. *J. Catal.* **2007**, *251*, 239−243.
(8) Kim, J.; Fang, B.; Yoon, S.; Yu, J. *Appl. Catal., B* **2009**, *88*, 368−375.
(9) Ji, Q. M.; Yoon, S. B.; Hill, J. P.; Vinu, A.; Yu, J. S.; Ariga, K. *J. Am. Chem. Soc.* **2009**, *131*, 4220−4221.
(10) Ariga, K.; Vinu, A.; Yamauchi, Y.; Ji, Q.; Hill, J. P. *Bull. Chem. Soc. Jpn.* **2012**, *85*, 1−32.
(11) Nishihara, H.; Kyotani, T. *Adv. Mater.* **2012**, *24*, 4473−4498.
(12) Chuenchom, L.; Kraehnert, R.; Smarsly, B. M. *Soft Matter* **2012**, *8*, 10801−10812.
(13) Roriguez-Reinoso, F. In *Introduction to Carbon Technology*; Marsh, H., Heintz, E. A., Rodriguez-Reinoso, F., Eds; Universidad de Alicante: Alicante, Spain, 1997; p 35.
(14) Corma, A. *Chem. Rev.* **1997**, *97*, 2373−2420.
(15) MacLachlan, M. J.; Aroca, P.; Coombs, N.; Manners, I.; Ozin, G. A. *Adv. Mater.* **1998**, *10*, 144−149.
(16) Norris, D. J.; Vlasov, Y. A. *Adv. Mater.* **2001**, *13*, 371−376.
(17) Su, F. B.; Zhao, X. S.; Wang, Y.; Wang, L. K.; Lee, J. Y. *J. Mater. Chem.* **2006**, *16*, 4413−4419.
(18) Nieto-Márquez, A.; Romero, R.; Romero, A.; Valverde, J. L. *J. Mater. Chem.* **2011**, *21*, 1664−1672.
(19) Deshmukh, A. A.; Mhlanga, S. D.; Coville, N. J. *Mater. Sci. Eng., R* **2010**, *70*, 1−28.
(20) Lamond, T. G.; Marsh, H. *Carbon* **1963**, *1*, 293−302.
(21) Hu, Z.; Srinivasan, M. P.; Ni, Y. *Adv. Mater.* **2000**, *12*, 62−65.
(22) Kyotani, T. *Carbon* **2000**, *38*, 269−286.
(23) Pekala, R. W. *J. Non-Cryst. Solids* **1992**, *145*, 90−98.

(24) Ozaki, J.; Endo, N.; Ohizumi, W.; Igarashi, K.; Nakahara, M.; Yoshida, S.; Iizuka, T. *Carbon* **1997**, *35*, 1031−1033.
(25) Chen, X. C.; Kierzek, K.; Jiang, Z. W.; Chen, H. M.; Tang, T.; Wojtoniszak, M.; Kalenczuk, R. J.; Chu, P. K.; Borowiak-Palen, E. *J. Phys. Chem. C* **2011**, *115*, 17717−17724.
(26) Hu, M.; Reboul, J.; Furukawa, S.; Torad, N. L.; Ji, Q. M.; Srinivasu, P.; Ariga, K.; Kitagawa, S.; Yamauchi, Y. *J. Am. Chem. Soc.* **2012**, *134*, 2864−2867.
(27) Yoon, S.; Sohn, K.; Kim, J.; Shin, C.; Yu, J.; Hyeon, T. *Adv. Mater.* **2002**, *14*, 19−21.
(28) Li, Y.; Yang, Y.; Shi, J.; Ruan, M. *Microporous Mesoporous Mater.* **2008**, *112*, 597−602.
(29) Bruce, P. G.; Scrosati, B.; Tarascon, J.-M. *Angew. Chem., Int. Ed.* **2008**, *47*, 2930−2946.
(30) Wakihara, M. *Mater. Sci. Eng., R* **2001**, *33*, 109−134. (b) Noel, M.; Suryanarayanan, V. *J. Power Sources* **2002**, *111*, 193−209.
(31) Zhou, H. S.; Zhu, S. M.; Hibino, M.; Honma, I.; Ichihara, M. *Adv. Mater.* **2003**, *15*, 2107−2111.
(32) Hu, Y. S.; Adelhelm, P.; Smarsly, B. M.; Hore, S.; Antonietti, M.; Maier, J. *Adv. Funct. Mater.* **2007**, *17*, 1873−1878.
(33) Ryoo, R.; Joo, S. H.; Kruk, M.; Jaroniec, M. *Adv. Mater.* **2001**, *13*, 677−681.
(34) Jun, S.; Joo, S. H.; Ryoo, R.; Kruk, M.; Jaroniec, M.; Liu, Z.; Ohsuna, T.; Terasaki, O. *J. Am. Chem. Soc.* **2000**, *122*, 10712−10713.
(35) Wang, X. Q.; Lee, J. S.; Tsouris, C.; DePaoli, D. W.; Dai, S. *J. Mater. Chem.* **2010**, *20*, 4602−4608.
(36) Liang, C. D.; Dai, S. *J. Am. Chem. Soc.* **2006**, *128*, 5316−5317.
(37) Meng, Y.; Gu, D.; Zhang, F. Q.; Shi, Y. F.; Cheng, L.; Feng, D.; Wu, Z. X.; Chen, Z. X.; Wan, Y.; Stein, A.; Zhao, D. Y. *Chem. Mater.* **2006**, *18*, 4447−4464.
(38) Fulvio, P. F.; Mayes, R. T.; Wang, X.; Mahurin, S. M.; Bauer, J. C.; Presser, V.; McDonough, J.; Gogotsi, Y.; Dai, S. *Adv. Funct. Mater.* **2011**, *21*, 2208−2215.
(39) Stöber, W. *J. Colloid Interface Sci.* **1968**, *26*, 62−69.
(40) Zhang, W. M.; Hu, J. S.; Guo, Y. G.; Zheng, S. F.; Zhong, L. S.; Song, W. G.; Wan, L. J. *Adv. Mater.* **2008**, *20*, 1160−1165.
(41) Lou, X. W.; Yuan, C.; Archer, L. A. *Small* **2007**, *3*, 261−265.

NOTE ADDED AFTER ASAP PUBLICATION

This paper was published ASAP on April 5, 2013. An additional reference was added to the paper, and the corrected version was reposted on April 9, 2013.